The International Journal of Advanced Manufacturing Technology (2018) 99:3123–3132
https://doi.org/10.1007/s00170-018-2600-y

ORIGINAL ARTICLE

Study on self-restrained explosive welding with high energy efficiency

Ming Yang[1] · Honghao Ma[1,2] · Zhaowu Shen[1]

Received: 27 April 2018 / Accepted: 15 August 2018 / Published online: 19 September 2018

Abstract
An innovative explosive welding technology, self-restrained explosive welding (SREW), was studied in this work. Compared to the conventional method, the new technology significantly increased the energy efficiency of explosives and produced less toxic and greenhouse gas. Moreover, it was able to obtain three or more welded plates all at once, and the motion of the plates was restrained by each other. Welding employing SREW method for a three-layer setup and two five-layer setups was conducted with different initial parameters. The dynamic parameters during the collision process were obtained theoretically and experimentally, and the welding quality was evaluated through optical metallographic observation. The results showed that the motion of all the welded plates was well restrained using this method, and the explosive consumption of a five-layer setup was reduced by 63% compared to the conventional method, when getting the same bonding quality and numbers of welded plates. The measured impact velocity values were found to be slightly lower than the calculated ones. According to microstructure analyses, excellent bonding interfaces were obtained through SREW method when employing suitable welding parameters.

Keywords Explosive welding · Self restraint · Energy efficiency · Environmental protection

1 Introduction

Explosive welding, a well-known solid state method for joining various metal materials, employs intense explosive energy to make metals produce a high-speed oblique collision and achieve metallurgical bond [1, 2]. This technology is characterized by good bonding quality and capability to directly join a wide variety of combinations of metals that may not be welded by any other techniques [3–5]. Up to now, more than 260 various similar and dissimilar metals and alloy combinations have been successfully welded using this technology [6]. The corrosion or wear resistance, thermal conductivity, or even anti-friction properties of composite materials produced by explosive welding are greatly improved [7]. In addition, explosive welding is capable of joining metals with large surface areas and keeping the physical and chemical properties of the wrought parent components unchanged [7].

Explosive welded products have been widely applied in both chemical and nuclear industries [5]. Because of the large demands for the welded plates, the explosive consumption is huge. Nonetheless, the earlier studies on explosive welding were mostly focused on the manufacturing procedures [8, 9], weldability window [10], and bonding properties for various types of joined metals [11–14]. There were few studies on energy efficiency of explosives and environmental protection. The conventional explosive welding (CEW) setup (Fig. 1) only takes advantage of the energy released by one side of explosive sheet. Amounts of energy are released freely in the form of air shock wave, which leads to big wastage of explosive energy and serious secondary pollution. Some researchers [15–18] employed underwater explosive welding technique to join easily damaged metals, and found that more ideal impact velocity of flyer plates was obtained due to that the shock waves exerting on flyer plates were adjusted by water. Meanwhile, explosion noise and dust were significantly reduced since amount of energy was absorbed by water. A double-sided explosive welding (DSEW) setup (Fig. 2) was proposed to increase the energy efficiency of explosives, in which less explosives could obtain two composite plates simultaneously [19, 20]. However, the high-speed uncontrollable motion of the DSEW plates may damage the products and cause

✉ Ming Yang
ym1991@mail.ustc.edu.cn

[1] CAS Key Laboratory of Mechanical Behavior and Design of Materials, Department of Modern Mechanics, University of Science and Technology of China, Hefei 230027, Anhui, China

[2] State Key Laboratory of Fire Science, University of Science and Technology of China, Hefei 230026, Anhui, People's Republic of China

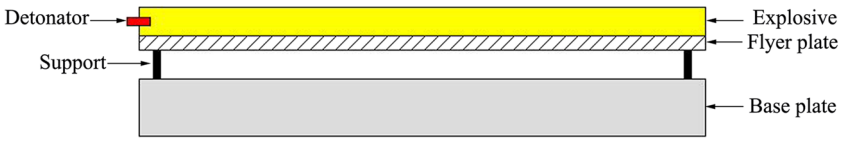

Fig. 1 The conventional explosive welding (CEW) setup

security risks, which make the direct application of DESW impossibility.

In present work, a self-restrained explosive welding (SREW) setup (Fig. 3) was proposed to improve energy efficiency of explosives and restrict the flight of the welded plates. In addition, water was used for covering the outer explosive sheet to reduce the dust. Steels were chosen as a model system since the broad application prospects and the physical and mechanical properties were well known [21, 22]. Welding of no. 45 steel to Q235 steel and SUS304 stainless steel to Q235 steel was carried out through SREW method, and the experimental results were analyzed by explosive welding window.

2 Weldability window

Reasonable selection of explosive welding parameters is necessary for good welding quality [10, 23]. There are three main dynamic parameters during collision process, i.e., collision angle β, collision point velocity v_c, and impact velocity v_p, however, they are related to each other for certain geometric relationships and only two of them are independent. Thus, any two of the dynamic parameters are capable of constituting a weldability window in the same plane. In this study, the collision point velocity v_c and collision angle β were selected to calculate the weldability window.

In order to make impact pressure at bonding interfaces exceed the yield stress of the materials to promote plastic deformation, the impact velocity of flyer plates must be larger than the lower limit of impact velocity. For welding of similar metallic materials, the lower limit of impact velocity can be calculated by the following formula [24]:

$$v_{\mathrm{pmin}} = \left(\frac{\sigma_b}{\rho}\right)^{1/2} \tag{1}$$

where σ_b is the tensile strength and ρ is the density of the flyer plate.

There were two different definitions proposed by Wittman [25] and Deribas [26] about upper limit of collision angle. For the former, the limit was defined to avoid producing a continuous interfacial melted zone between the metal materials. According to the thermophysical properties of the welded materials, the below equation was proposed to describe the upper limit [25].

$$\sin\left(\frac{\beta}{2}\right) = \frac{1}{N}\frac{(T_m c)^{1/2}}{2v_c^2}\left(\frac{kc_p c}{\rho h}\right)^{1/4} \tag{2}$$

where all parameters are referred to the material properties of the flyer plate, and N is a constant factor for steel taking the value of 0.062 [27], T_{m} the melting temperature, c the sonic speed, k the thermal conductivity, c_p the specific heat capacity, and h the thickness.

Deribas [26] accepted the interfacial melted zone that was not allowed to occur in Wittman's upper limit, and defined the boundary by determining the condition that the time for solidification of the melted zone should be less than the time for tensile wave to reach the interface. Therefore, there is no welding joint forming on the top of the boundary calculated by Deribas, and welding occurs with interfacial melted zones in the region between the two upper boundaries. Deribas [26] calculated the upper boundary by the following equation.

$$\sin\left(\frac{\beta}{2}\right) = \left(\frac{E}{6\rho(1-2\nu)}\right)^{\frac{1}{2}}\frac{1}{h^{0.25}v_c^{1.25}} \tag{3}$$

where E and ν are the elastic modulus and Poisson's ratio of the flyer plate respectively.

There is a lower limit of collision point velocity for predicting the laminar–turbulent flow transition of the welded materials. This limit also defines the transition from straight to wavy interfaces between the flyer and base plates. Wavy interfaces can be obtained when the collision point velocity is larger than the lower limit. Cowan et al. [28] defined the lower limit of collision point velocity with hydrodynamic analogy.

$$v_{\mathrm{cmin}} = \left[\frac{2R_e(H_1+H_2)}{\rho_1+\rho_2}\right]^{1/2} \tag{4}$$

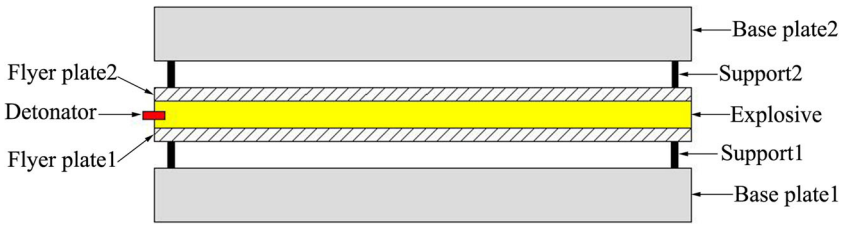

Fig. 2 The double-sided explosive welding (DSEW) setup

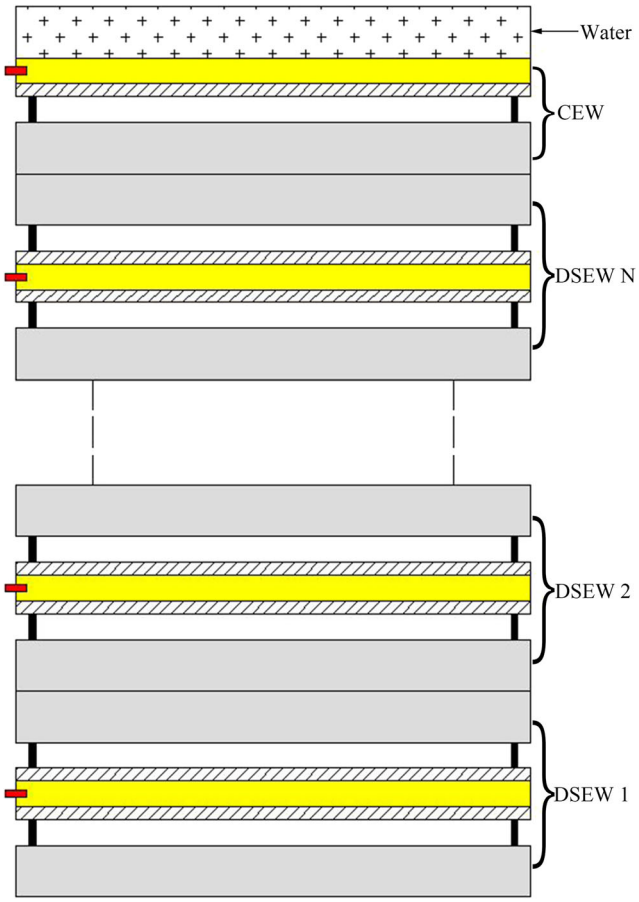

Fig. 3 The self-restrained explosive welding (SREW) setup

where *Re* is a critical Reynolds number taking values of 10.5 [27] and H_1 and H_2 are the Vickers hardness numbers of the flyer and base plates respectively.

The upper limit of collision point velocity is related to the formation of a jet at the collision point. For this reason, Walsh et al. [29] proposed that the collision point velocity should not be larger than the sound speed of the welded materials. However, this limit is not enough to meet the condition that jetting and consequently welding occur. A minimum collision angle is also required to satisfy that impact pressure is high enough to drive the interface metals into a jet. Thus, the upper limit of the collision point velocity v_c was calculated as a function of collision angle β [30].

$$v_c = \frac{\beta}{10} + 5.5 \tag{5}$$

The material property parameters involved to the calculations are given in Table 1. Welding window of no. 45 steel to Q235 steel and SUS304 stainless steel to Q235 steel were developed based on Eqs. (1)–(5) and shown in Figs. 4 and 5 respectively. The parameters used in this paper are also shown in Figs. 4 and 5.

3 Experiment

3.1 Experiment methods

Figure 3 shows the schematic diagram of SREW. This arrangement is composed of one or more setups of DSEW (Fig. 2) and one setup of CEW (Fig. 1). The setups of DSEW are symmetric to the explosive sheet, which are stacked on top of each another in sequence. The setup of CEW is placed on the top of all DSEW setups. In order to mitigate the secondary pollution and improve explosion energy efficiency, water with the same mass as a flyer plate is placed on the top of the CEW setups. For investigating the restricting effect of the SREW method on the welded plate, two groups of tests were carried out in a cylindrical explosion vessel respectively adopting a three-layer setup (one setup of DSEW and one setup of CEW) and a five-layer setup (two setups of DSEW and one setup of CEW). The diameter and length of the vessel are 2.5 m and 5 m, and the inner wall of the vessel was coated with plastic film. We judged the restricting effect by sign of impact between welded plates and inter wall of the vessel. A test using sand soil to restrict the motion of the DSEW plate was also conducted for a comparison. As shown in Fig. 6, the thickness and density of the sand soil are 100 cm and 1.8 g/cm^3. This test was carried out in open space, and we evaluated the restricting effects by recording the flight distance of the upper welded plate. In the three tests, the welding parameters were selected close to the upper limit of the welding window to obtain the maximal velocity of the welded plate. Thus, the motion of the welded plate is the hardest to be restricted in this condition, which makes the experiments more convincing.

A test with five-layer setup was carried out to study the welding property of the SREW method, and a test using the CEW method was also conducted for a comparison. For the two tests, the welding parameters were selected suitable for

Table 1 Selected material parameters used for calculating welding window

Material	ρ [kg m^{-3}]	H_v [Mpa]	c [m s^{-1}]	σ_b [Mpa]	T_m [°C]	K [w/(m °C]	c_p [J/(kg °C]	E [Gpa]	ν
Q235	7850	1300	6000	405	1493	38	500	210	0.27
No. 45	7850	1900	5200	600	1495	38	500	210	0.27
SUS304	7930	1700	4500	560	1454	22	500	194	0.30

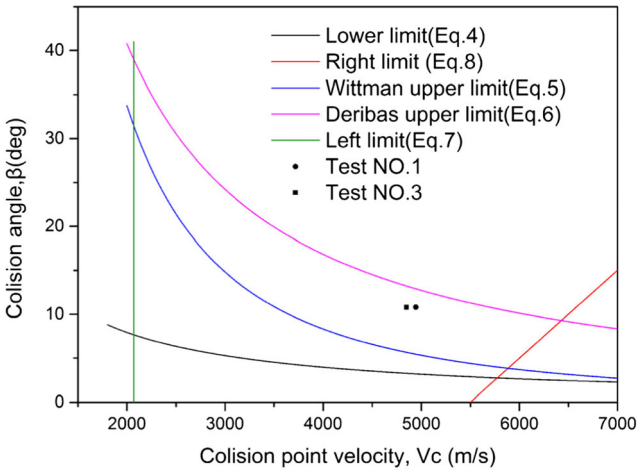

Fig. 4 Welding window of no. 45 steel/Q235 steel for explosive cladding with selected parameters

explosive welding, so good bonding interfaces were expected to be obtained.

Figure 7 illustrates the detonation velocity and dynamic parameter measurements, in which the detonation velocity was measured by recording the time interval between two probes (The chronometer is 2BS-110 with a time resolution of 0.1 μs). Four probes were employed for each of the experiments, and the average detonation velocity was determined. The dynamic parameters were obtained by measuring the triggering time of three sensors. After the explosive initiation, the explosion pressure drove the flyer plate downward as the detonation wave moved forward. As shown in Fig. 7, during the continuous collision between the flyer plate and base plate, sensors A, B, and C (the same three PVDF piezoelectric gage with thickness of 50 μm and maximum response frequency of 1000 MHz) were triggered sequentially, and the triggering time was recorded by an oscilloscope with a time resolution of 1 ns (Tektronix MDO4104C). Figure 8 shows a typical oscillogram obtained with this technique

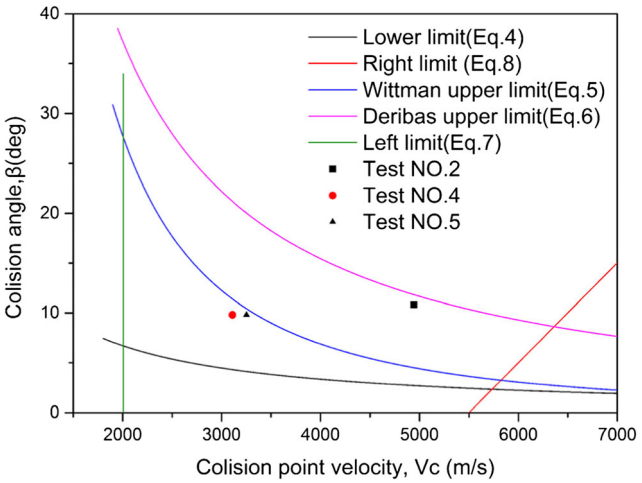

Fig. 5 Welding window of SUS304 stainless steel/Q235 steel for explosive cladding with selected parameters

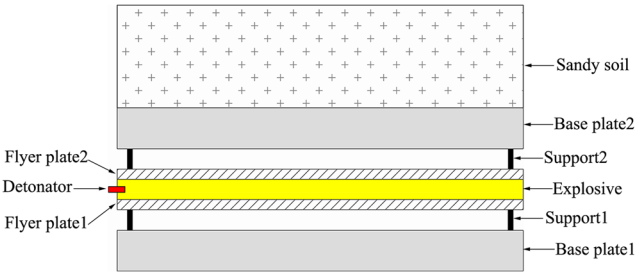

Fig. 6 Schematic diagram of DSEW using sandy soil to restrict the upper welded plate

(test no. 4). The collision point velocity v_c is determined by the following equation:

$$v_c = \frac{s_1 + s_2}{t_1 + t_2} \tag{6}$$

where s_1 is the horizontal distance between A and B, s_2 is the horizontal distance between B and C, t_1 is the triggering time interval of sensor A and B, and t_2 is the triggering time interval of sensor B and C.

The collision angle β is expressed as

$$\beta = \tan^{-1}\left(\frac{h}{s_1 - v_c t_1}\right) \tag{7}$$

where h is the vertical distance between B and A (The height of A and C is equal).

After calculating v_c and β, the impact velocity v_{pe} can be calculated by the following equation:

$$v_{pe} = 2v_c \sin(\beta/2) \tag{8}$$

The conditions of the measurements were designed to be the same with the welding conditions, and the initial parameters for the measurements are listed in Table 2.

The parallel setup geometry located on a steel anvil was employed for all the experiments. All detonators were located at the same position of each explosive sheet and initiated simultaneously. After welding, the specimens were cut parallel to detonation direction, and the cross-sections of which were

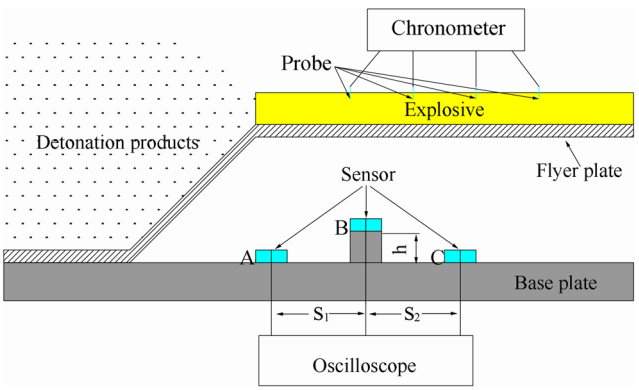

Fig. 7 Diagram of detonation velocity and impact velocity measurement

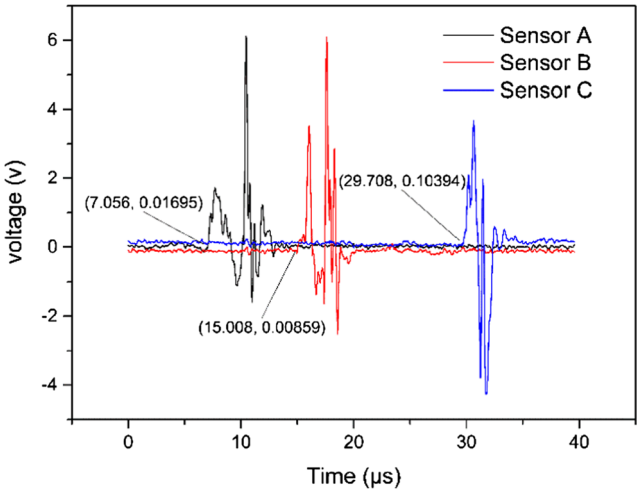

Fig. 8 Typical example of a result used to determine the impact velocity

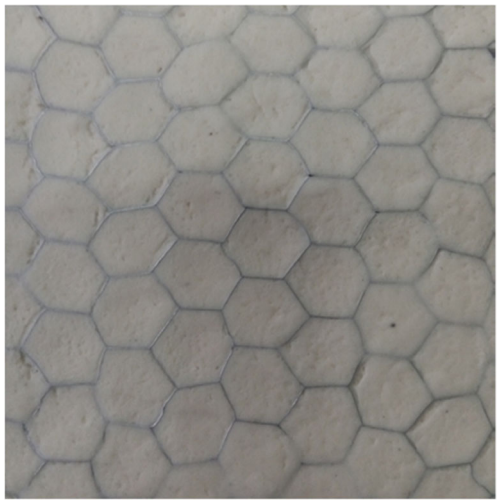

Fig. 9 Honeycomb structure explosive

ground with emery papers up to no. 3000 and polished to 1 um by diamond paste. Then, the welded plates were etched by etchant consisting of 3 mL HNO_3 and 97 mL anhydrous alcohol.

3.2 Experiment materials

The flyer and base plates employed in the three-layer setup and DSEW setup were made of no. 45 steel and Q235 steel. SUS304 stainless steel and Q235 steel plates were employed as flyer and base plates respectively for the two groups of five-layer setup and the conventional setup. The dimensions of the flyer and base plates were 300 mm × 150 mm × 2 mm and 300 mm × 150 mm × 20 mm respectively in all the experiments, and their surfaces were used as received. The physical and mechanical properties of the flyer and base plates are given in Table 1.

Honeycomb structure explosives consisting of aluminum honeycomb filled with emulsion explosive were employed as explosive materials, which can improve the mechanical strength of the explosive and accurately control the height and uniformity of the explosive. As shown in Fig. 9, the thickness of aluminum foil was 60 μm and the side length of the regular hexagon cell was 8 mm. The components of the emulsion matrix are presented in Table 3. Hollow glass microballoons were chosen as the sensitizer with mass fraction of 4% and 15%.

4 Results and discussion

For all the SREW tests, no sign of impact was found on internal surface of the vessel, and all the welded plates nearly remained in the initial position (no more than 1.5 m), which demonstrated that the flight of all the welded plates was well restrained using this method. Since the same collision angle and collision point velocity were designed for every flyer plate, the flight velocity of two adjacent welded plates was the same size but in the opposite directions. Therefore, the motion of the two adjacent welded plates was constrained by impacting with each other. Because both the upper and lower sides of explosive sheet were constrained, the energy released freely was reduced and energy efficiency was increased. Moreover, covering water was vaporized and scattered in the air, which mitigated the explosion smoke and dust. While for the DSEW test, although the thickness of the sand soil was as high as 100 cm, the result showed that the upper welded plate traveled up to about 50 m away from the initial position. Obviously, the restricting effect is unsatisfactory using this

Table 2 The explosive welding and dynamic parameter measurements for different experiments

Test no.	Experimental method	S_1 (mm)	S_2 (mm)	h (mm)	x_0 (mm)	x_1 (mm)	ρ (g cm^{-3})
1	Three-layer setup	34.8	35.4	1.98	10	8	1.18
2	Five-layer setup	35.2	35.2	1.94	10	8	1.18
3	DSEW setup	34.8	35.5	1.96	10	8	1.18
4	Five-layer setup	35.7	35.0	1.92	10	8	0.80
5	Conventional setup	35.6	35.0	1.94	16	8	0.80

Note: x_0 is the explosive thickness, x_1 is the stand-off distance between flyer and base plate, and ρ is the explosive density

Table 3 Component of the emulsion matrix

Component	NH_4NO_3	$NaNO_3$	H_2O	$C_{18}H_{38}$	$C_{24}H_{44}O_6$	$C_{12}H_{26}$
Mass fraction	75%	10%	8%	4%	2%	1%

way. Considering that this method can also lead to other problems such as added costs, covering material shortage et al., so it is not an ideal way to restrict the motion of the upper welded plate.

Figure 10 shows the welded plates of SREW from test no. 4. Five composite plates were obtained through one shot, which is helpful to improve the work efficiency and save explosion place. As shown in Fig. 10, no macroscopic defect was observed, and the ultrasonic test results showed that all five welded plates were 100% bonded. In addition, the welded plate produced by CEW also achieved 100% bonding, which indicated that the welding parameters of the two tests were reasonable.

4.1 Impact velocity of flyer plate

For the setups of CEW with a covering for explosives, the impact velocity v_{pg} is calculated from the Gurney equation adapted for asymmetric sandwich configurations [31].

$$v_{pg} = \sqrt{2E}\left[\frac{1+A^3}{3(1+\mathrm{A})} + \frac{N}{C}A^2 + \frac{M}{C}\right]^{-1/2} \tag{9}$$

where E is the Gurney energy and N, C, and M are the mass per unit of area of the covering, the explosive, and the flyer plate, respectively. N is equal to 0 for CEW without covering.

The A is determined by the formula below [31]:

$$A = \frac{1+2\frac{M}{C}}{1+2\frac{N}{C}} \tag{10}$$

For the two welding methods of DSEW and SREW, the covering is also a flyer plate, which is the same as the plate on the bottom of the explosive sheet, that is, $N = M$. So we obtain the Gurney impact velocity of this case from simplifying Eq. (9).

$$v_{pg} = \sqrt{2E}\left[\frac{1}{3} + 2\frac{M}{C}\right]^{-1/2} \tag{11}$$

Based on energy conservation, a calculation formula of Gurney energy was given [32].

$$E = \frac{1}{\gamma^2 - 1}\left(\frac{\gamma}{\gamma+1}\right)^{\gamma} {v_d}^2 \tag{12}$$

where γ is the polytropic exponent of detonation products, and the value for emulsion explosive is equal to 2.5.

The Gurney velocity of flyer plates can be calculated by substituting Eq. (12) into Eqs. (9) and (11). However, the value of the impact velocity v_{pg} predicted by Gurney equation corresponds to the terminal velocity, it is necessary to take into consideration its acceleration at such a short stand-off distance of 8 mm. Based on Lagrange's principle, the following equation was proposed to describe the acceleration history for asymmetric sandwich configurations [33]:

$$v_{pc} = v_{pg}\left[1 - \left(\frac{x_0}{x_0 + (1+A)x_1}\right)^{\gamma-1}\right]^{1/2} \tag{13}$$

where x_0 is the initial thickness of explosives and x_1 is the displacement of the flyer plate.

The calculated (according to the aforementioned procedure) Gurney velocity v_{pg} and impact velocity v_{pc}, the measured detonation velocity v_d, collision point velocity v_c, collision angle β, and impact velocity v_{pe} are listed in Table 4.

It is generally recognized that the collision point velocity is equal to the detonation velocity of explosives for parallel setup geometry. As listed in Table 4, the measured detonation velocity v_d and collision point velocity v_c are nearly equal, which verified the reliability of the experiment. For impact velocity, the maximum error of the calculated and measured value is not more than 8%, which proved the effectiveness of the calculation. The measured value v_{pe} is slightly lower than the calculated value v_{pc}, which could be attributed to air and support column that influence the impact velocity with a negative manner. Table 4 also shows that the similar impact velocity of test no. 4

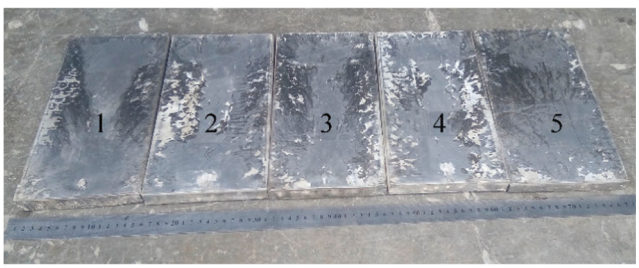

Fig. 10 Welded plates of SREW from test no. 4

Table 4 The calculated and measured results for different experiments

Test no.	v_d (m/s)	v_c (m/s)	β (°)	v_{pe} (m/s)	v_{pc} (m/s)	v_{pg} (m/s)
1	4919	4944	10.8	931	1001	1147
2	4980	4923	11.4	980	1013	1161
3	4880	4848	10.8	925	993	1138
4	3219	3110	9.8	534	549	629
5	3283	3253	9.8	557	597	631

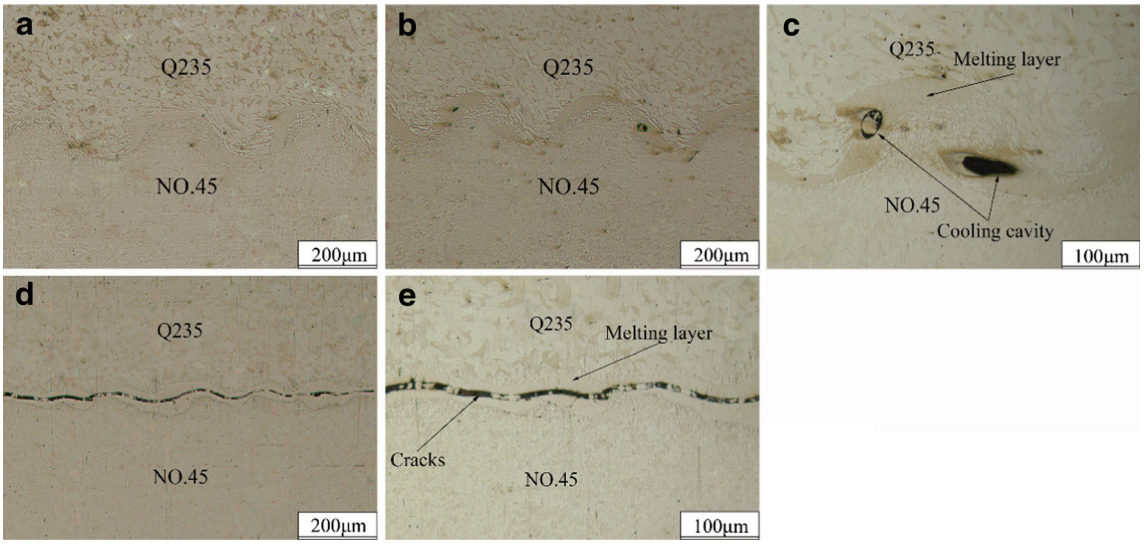

Fig. 11 Morphology of weld interface for test no. 1. **a**, **c** The lower plate of DSEW. **b** The upper plate of DSEW. **d**, **e** The plate of CEW with covering

and test no. 5 were obtained; for test no. 4 (SREW of five-layer setup), three explosive sheets with the thickness of 10 mm produced five welded plates, while for test no. 5 (setup of CEW), one explosive sheet with the thickness of 16 mm only obtained one welded plate. Compared to the CEW method, the explosive consumption of test no. 4 was reduced by 63%, when getting the same welding condition and numbers of welded plates.

4.2 Microscopic observations

Figure 11 shows the microstructure of as-welded specimen interfaces for test no. 1. As shown in Fig. 11a, b, the bonding interfaces of the two welded plates from DSEW are exactly similar, which could be attributed to that the flyer plates on both sides of the explosive sheet were subjected to the same

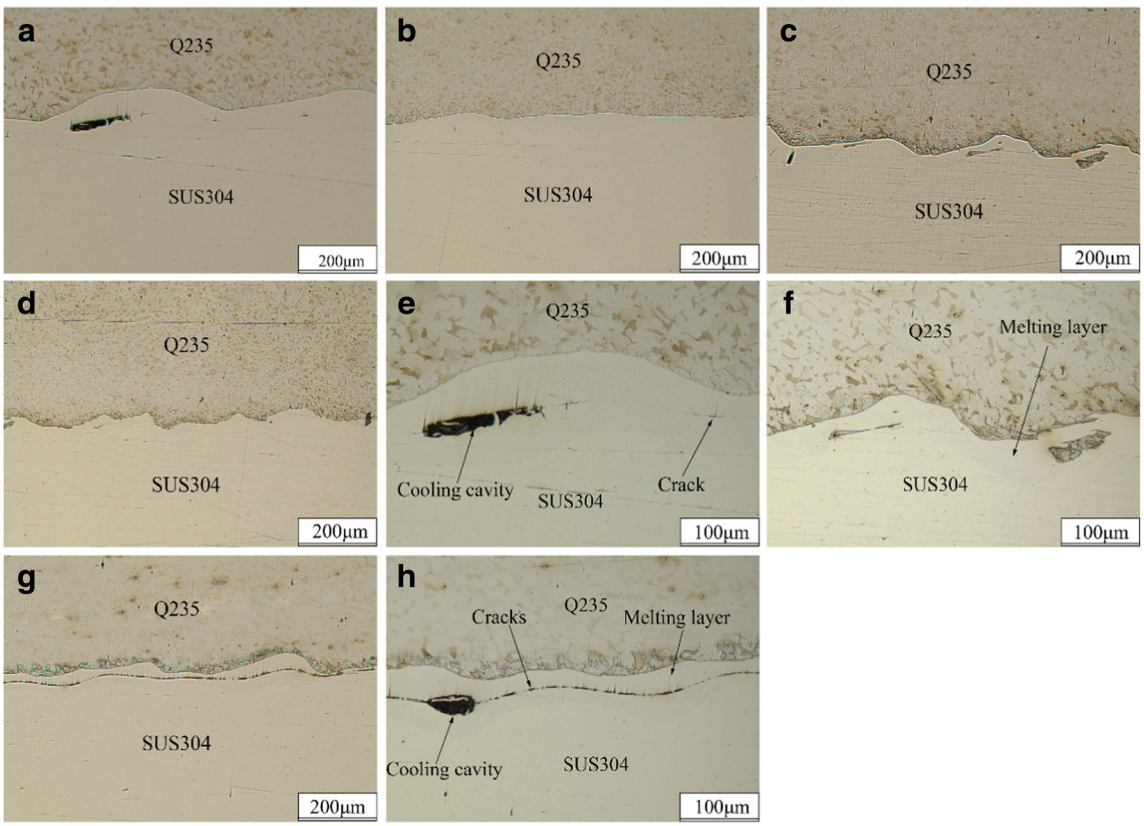

Fig. 12 Morphology of weld interface for test no. 2. **a**, **e** The lower plate of DSEW 1. **b** The upper plate of DSEW 1. **c**, **f** The lower plate of DSEW 2. **d** The upper plate of DSEW 2. **g**, **h** The plate of CEW with covering.

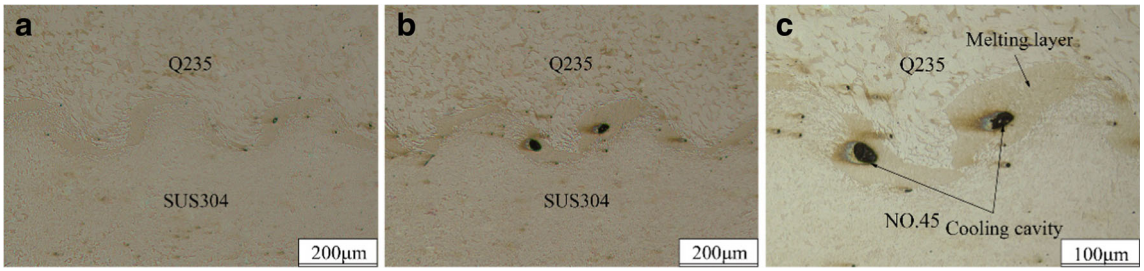

Fig. 13 Morphology of weld interface for test no. 3. **a** The lower plate of DSEW. **b**, **c** The upper plate of DSEW

loading. According to the welding window (Fig. 4), the welding condition was placed close to the upper boundary calculated by Deribas [26]; therefore, waviness with melted zones was expected to be formed at the bonding interfaces. Metallographic examination of the welded plate confirmed the prediction. The regular wave morphology with discontinuous melted zones was observed at the bonding interfaces, as illustrated in Fig. 11a, b. The average wavelength and amplitude of the wave are 515 μm and 170 μm, respectively, and the thicknesses of the melted zones are in the range of 0–90 μm. It is generally recognized that dissipated energy of the impacting plates in the form of heat increasing leads to the melted zones [34]. The materials near vortexes of the bonding interface are heated the most [35], so the thickest melted zones are usually formed in those regions. Typical defects such as cooling cavity and cracks in the vortices due to solidification can be seen in Fig. 11c, which can deteriorate the properties of the bonding interface [36]. For the welded plate from CEW, the microscopic result shows that irregular waves with continuous melted zones were formed at the bonding interface (see Fig. 11d, e). Unlike the DSEW, there are almost continuous cracks at the middle of the melted zones, which could be attributed to tensile wave from the free surface. For the CEW setup, the compression wave produced by the collision between the flyer and base plates is changed to a tensile wave by the free surface reflection. When the tensile wave reaches the interface, the melting zones of the bonding interfaces have not completely solidified, so which are separated by the tensile wave. While for the DSEW setup, the movement of detonation products is restricted by the two flyer plates, so the wave impedance of detonation products is larger than that of CEW setup when the compression wave to reach the free surface. As a result, the

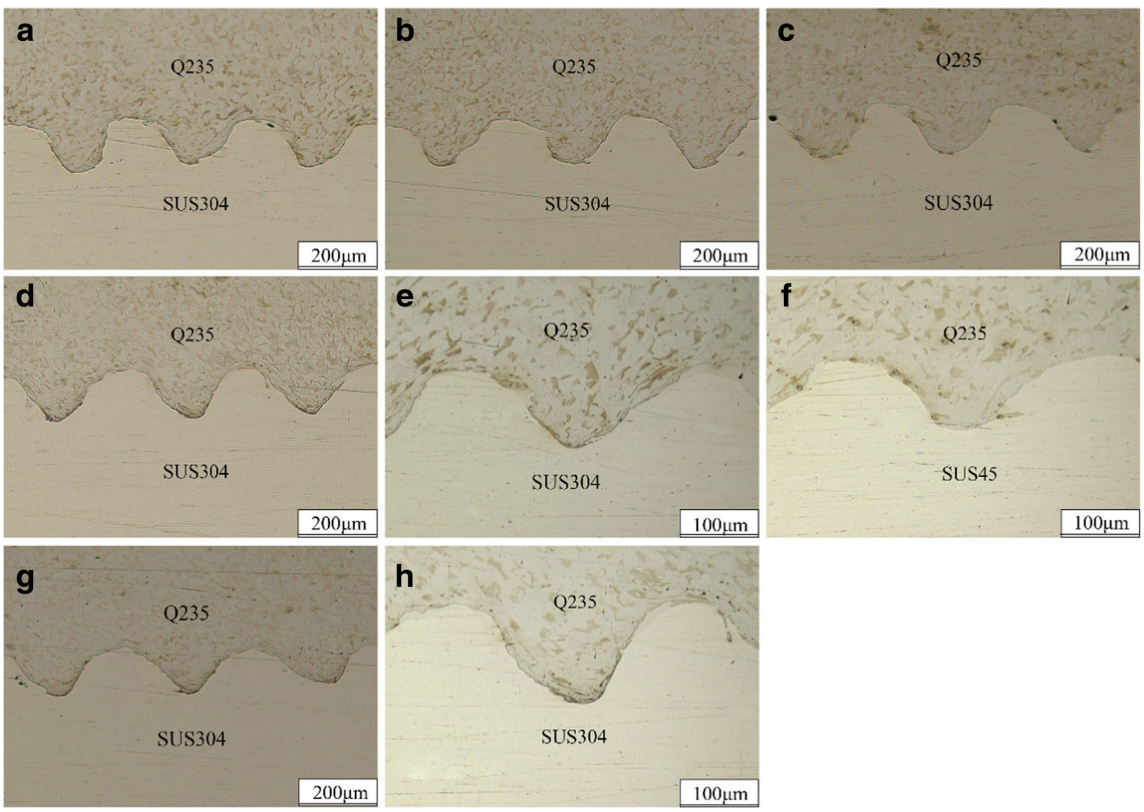

Fig. 14 Morphology of weld interface for test no. 4. **a**, **e** The lower plate of DSEW 1. **b** The upper plate of DSEW 1. **c**, **f** The lower plate of DSEW 2. **d** The upper plate of DSEW 2. **g**, **h** The plate of CEW with covering

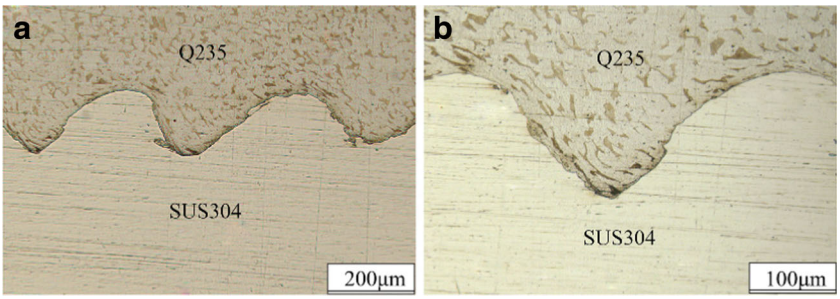

Fig. 15 Morphology of weld interface for test no. 5. **a**, **b** The CEW plate

amplitude of the reflected tensile wave is less than that of CEW setup. When the tensile wave reaches the bonding interface, which is too weak to separate the melting zones.

Morphologies of the bonding interfaces for test no. 2 are shown in Fig. 12. According to Fig. 12a–f, wave interfaces with melted zones are obtained for the two groups of DSEW, while for the CEW, cracks are observed at the middle of the melted zone, as shown in Fig. 12g, h. The results are consistent with those of test no. 1, and the detailed analysis has been done before. Since the welding dynamic parameters of the two tests were designed to be the same and similar bonding properties were obtained, which indicated that such method had satisfying reproducibility. Figure 13 shows the metallographic structures of specimen interfaces from test no. 3, where the interface morphologies are consistent with those of DSEW from test no. 1. This is due to the fact that the same welding parameters were selected for the two tests.

Figure 14 shows the metallographic structures of as-welded specimen interfaces for the test no. 4. Unlike test no. 1–3, the welding dynamic parameters of this test were placed within the welding window (Fig. 5). Thus, the welding window predicts that sound bonding with wave morphology will be obtained. Metallographic examination of this test is consistent with the prediction (see Fig. 14). The average wavelength and amplitude of the waves are 440 μm and 160 μm respectively, and there are almost no melted zone, crack, and loose like "cavity" in the bonding interface, which shows that an excellent connection between the welded materials was created. Similar bonding interfaces are obtained for the welded plates produced by DSEW and CEW in this test, which is attributed to relatively low impact velocity. Thus, the melting zone of bonding interface is completely solidification when the tensile wave to reach the interface.

The optical figures of test no. 5 are shown in Fig. 15. As what mentioned before, the explosive consumption of test no. 4 is 63% lower than that of test no. 5. However the similar collision point velocity and collapse angle of the two groups of tests were obtained (see Table 4). Thus, consistent bonding interfaces were obtained for the two groups of tests, as shown in Fig. 14 and Fig. 15. This indicated that SREW method can achieve the same results with less cost than the CEW method.

5 Conclusions

In this study, a SREW technology was presented. Using this technology, three groups of experiments were systematically investigated. The following conclusions can be drawn:

1. Compared to the conventional method, the explosive consumption for SREW with a five-layer setup was reduced by 63%, when getting the same bonding quality and numbers of welded plate.
2. The SREW technology enables to obtain three or more composite plates through one shot, which is helpful to improve the work efficiency and save explosion place.
3. The ultrasonic tests and microstructure analyses indicated that excellent bonding interfaces were obtained through SREW technology when employing suitable welding parameters.
4. The measured impact velocity values are slightly lower than the calculated ones; however, the maximum error of all the tests is less than 8%.
5. The flight of all the welded plates was well restrained using SREW method; however, placing covering on top of the DSEW setup is not an ideal way to restrict the motion of the upper welded plate.

Funding information The reported research is supported by the China National Nature Science (no. 51674229 and no. 51374189) and Fundamental Research Funds for Central Universities (WK2480000002).

References

1. Kahraman N, Gülenç B (2005) Microstructural and mechanical properties of Cu–Ti plates bonded through explosive welding process. J Mater Process Technol 169(1):67–71
2. Akbari Mousavi SAA, Farhadi Sartangi PF (2009) Experimental investigation of explosive welding of cp-titanium/AISI 304 stainless steel. Mater Des 30(3):459–468
3. Acarer M, Demir B (2008) An investigation of mechanical and metallurgical properties of explosive welded aluminum-dual phase steel. Mater Lett 62(25):4158–4160

4. Wang B, Chen W, Li J, Liu Z, Zhu X (2013) Microstructure and formation of melting zone in the interface of Ti/NiCr explosive cladding bar. Mater Des 47(9):74–79
5. Fındık F (2011) Recent developments in explosive welding. Mater Des 32(3):1081–1093
6. Kacar R, Acarer M (2004) An investigation on the explosive cladding of 316L stainless steel-din-P355GH steel. J Mater Process Technol 152(1):91–96
7. Mendes R, Ribeiro JB, Loureiro A (2013) Effect of explosive characteristics on the explosive welding of stainless steel to carbon steel in cylindrical configuration. Mater Des 51(51):182–192
8. Sakhtemanian MR, Honarpisheh M, Amini S (2017) Numerical and experimental study on the layer arrangement in the incremental forming process of explosive-welded low-carbon steel/CP-titanium bimetal sheet. Int J Adv Manuf Technol 1(4):1–16
9. Mali VI, Bataev AA, Maliutina IN, Kurguzov VD, Bataev IA, Esikov MA, Lozhkin VS (2017) Microstructure and mechanical properties of Ti/Ta/Cu/Ni alloy laminate composite materials produced by explosive welding. Int J Adv Manuf Technol 12:1–10
10. Athar MM, Hoseini B, Tolaminejad (2015) Weldability window and the effect of interface morphology on the properties of Al/Cu/Al laminated composites fabricated by explosive welding. Mater Des 86:516–525
11. Bazarnika P, Adamczyk-Cieślaka B, Gałkab A, Płonkac B, Snieżekd L, Cantonie M, Lewandowskaa M (2016) Mechanical and microstructural characteristics of Ti6Al4V/AA2519 and Ti6Al4V/AA1050/AA2519 laminates manufactured by explosive welding. Mater Des 111:146–157
12. Guo X, Wang H, Liu Z, Wang L, Ma F, Tao J (2016) Interface and performance of clam steel/aluminum clad tube prepared by explosive bonding method. Int J Adv Manuf Technol 82(1–4):543–548
13. Bai QL, Zhang LJ, Xie MX, Yang HX, Zhang JX (2016) An investigation into the inhomogeneity of the microstructure and mechanical properties of explosive welded h62-brass/q235b-steel clad plates. Int J Adv Manuf Technol 90(5–8):1351–1363
14. Kaya Y, Kahraman N, Durgutlu A, Gülenç B (2017) Investigation of the microstructural, mechanical and corrosion properties of grade a ship steel-duplex stainless steel composites produced via, explosive welding. Metall Mater Trans A 48(8):3721–3733
15. Manikandan P, Lee JO, Mizumachi K, Mori A, Raghukandan K, Hokamoto K (2011) Underwater explosive welding of thin tungsten foils and copper. J Nucl Mater 418(1–3):281–285
16. Sun W, Li X, Yan H, Wang X (2012) An alternative thin-plate welding technology using underwater shock wave. J Adhes Sci Technol 26(10–11):1733–1743
17. Sun W, Li X, Yan H, Hokamoto K (2013) Effect of initial hardness on interfacial features in underwater explosive welding of tool steel SKS3. J Mater Eng Perform 23(2):421–428
18. Yu Y, Ma H, Zhao K, Shen Z, Cheng Y (2017) Study on underwater explosive welding of al-steel coaxial pipes. Cent Eur J Energ Mater 14(1):251–265
19. Miao G, Ma H, Shen Z, Yu Y (2014) Research on honeycomb structure explosives and double sided explosive cladding. Mater Des 63(2):538–543
20. Shi CG, Wang Y, Zhao LS, Hou HB, Ge YH (2015) Detonation mechanism in double vertical explosive welding of stainless steel/steel. J Iron Steel Res Int 22(10):949–953
21. Sathiya P, Aravindan S, Haq AN (2005) Mechanical and metallurgical properties of friction welded AISI 304 austenitic stainless steel. Int J Adv Manuf Technol 26(5–6):505–511
22. Reddy MG, Rao KS (2009) Microstructure and mechanical properties of similar and dissimilar stainless steel electron beam and friction welds. Int J Adv Manuf Technol 45(9–10):875–888
23. Li X, Ma H, Shen Z (2015) Research on explosive welding of aluminum alloy to steel with dovetail grooves. Mater Des 87:815–824
24. Stivers SW, Wittman RH (1975) Computer selection of the optimum explosive loading and welding geometry, igh energy rate fabrication. Proc Semin 5nd Int Symp 4(2):1–16
25. Wittman RH (1973) The influence of collision parameters on the strength and microstructure of an explosion welded aluminum alloy. The Use of Explosive Energy in Manufacturing, Proc of the 2nd Int Symp, Marianskie Lazni, Czechoslovakia 153–168
26. Deribas A (1972) Physics of explosive hardening and welding (in Russian) Nauka. Novosibirsk
27. Ribeiro JB, Mendes R, Loureiro A (2014) Review of the weldability window concept and equations for explosive welding. J Phys Conf Ser 500:052038
28. Cowan GO, Bergmann A (1971) Holtzman. Mechanism of bond zone wave formation in explosion-clad metals. Metall Mater Trans B Process Metall Mater Process Sci 2(11):3145–3155
29. Walsh J, Shreffler R, Willig F (1953) Limiting conditions for jet formation in high velocity collisions. J Appl Phys 24(3):349–359
30. Abrahamson GR (1961) Permanent periodic surface deformations due to a traveling jet. J Appl Mech 83:519–528
31. Zukas JA, Walters WP (1998) Explosive effects and applications. Springer, New York 5: 417; ISBN 978-1-4612-0589-0
32. Koch A, Arnold N, Estermann M (2002) A simple relation between the detonation velocity of an explosive and its gurney energy. Propellants Explos Pyrotech 27(6):365–368
33. Flis, William J (1994) A lagrangian approach to modeling the acceleration of metal by explosives. Southeastern Conference on Theoretical and Applied Mechanics
34. Hokamoto K, Izuma T, Fujita M (1993) New explosive welding technique to weld. Metall Trans A 24(10):2289–2297
35. Bataev I, Bataev A, Mali V, Bataev V, Balaganskii I (2014) Structural changes of surface layers of steel plates in the process of explosive welding. Met Sci Heat Treat 55(9–10):509–513
36. Lee WB, Bang KS, Jung SB (2005) Effects of intermetallic compound on the electrical and mechanical properties of friction welded Cu/Al bimetallic joints during annealing. J Alloy Compd 390(1–2):212–219